Summary of project OTKA PD 105364

Principal investigator: Tibor Guzmics

Introduction

During my proposal, textural analyses and optical microscopic study were carried out on the following rock samples: magnetite-carbonatite (Jacupiranga, Brazil), jacupirangite and afrikandite (Kerimasi, Tanzania), afrikandite (Kola, Russia), alkaline-xenoliths (Alcsútdoboz, Hungary). I have prepared 30 doubly-polished thin sections for petrographic analyses. The coexisting fluid and melt inclusions together with their petrographic relations to host minerals [nepheline, perovskite, clinopyroxene and melilite (Kerimasi); nepheline, perovskite and clinopyroxene (Kola) magnetite, calcite and apatite (Kerimasi and Jacupiranga); clinopyroxene and feldspar (Alcsútdoboz)] have been studied in detail. All rock samples studied contain primary melt inclusions. Mineral grains, containing the melt inclusions, were separated (n= 500) and fixed onto glass slabs, using super glue and, then polished onto their both sides.

Because of the large number of melt inclusions in studied samples, I decided focusing on a detailed study of melt inclusions and host rocks from Kerimasi (afrikandite, jacupirangite and calciocarbonatite) and Jacupiranga (magnetite-carbonatite) instead of submitting preliminary results of my textural observations from Kola and Alcsútdoboz to any journal. My decision has been also justified by an overall international interest in Gregory Rift Valley, especially in Kerimasi volcano.

Fulfilled analytical and experimental work

Kerimasi samples

Fourteen high-T (850-1050 ^{o}C) homogenization experiments on clinopyroxene-hosted carbonate melt inclusions (jacupirangite). 386 Raman point measurements on unheated clinopyroxene- (both exposed and non-exposed) and magnetite-hosted (exposed) melt inclusions together with the rock-forming minerals (jacupirangite). Fifty Raman point measurements on the bubble phases of heated melt inclusions, by using the combination of Raman and Linkam stage. Twenty Raman point measurements on the quenched melt phases. Heating and quenching experiments on 150 magnetite and 150 clinopyroxene grains containing melt inclusions (jacupirangite). Polishing these grains until exposure of the quenched melt inclusions. 200 SEM and 188 EMPA analyses on the quenched melt inclusions; 144 EMPA

analyses on the mineral phases (jacupirangite). One hundred and eighty LA-ICP-MS measurements on the afrikandite and calciocarbonatite rock samples, including their mineral phases and melt inclusions. Quantification of these analyses. Recording and evaluating four high resolution 3D Raman maps of carbonate melt inclusions hosted in clinopyroxenes from afrikandite and jacupirangite, including 320 Raman point measurements. Four FIB-SEM analyses of the previously Raman-mapped melt inclusions (one FIB-SEM run requires 100-130 steps, including 110 SEM and 110 BSE images together with 350 EDS spectra). Collecting of 30 Kikuchi-patterns from daughter minerals of melt inclusions. Evaluating of these data. Creating four 3D-FIB-SEM models and calculating volume ratio of the daughter minerals.

Magnetite-carbonatite, Jacupiranga

254 Raman point measurements on mineral phases and melt inclusions of magnetite-carbonatite. 300 SEM analyses on the previously Raman-detected and newly identified mineral phases. Evaluating of these data.

Results

All data collected from Kerimasi samples during my proposal together with our scientific results have been published/accepted in international journals (*Guzmics et al., 2012, 2015, Contrib Mineral Petrol; Káldos et al., 2015, Lithos*). A paper showing our results on Raman-FIB-SEM-3D modelling is under preparation. Publishing data from Jacupiranga samples is going on as well. Short scientific summaries of the latters can be found in the next sections. Results of our investigations have been shown in 10 times in international (*e.g.*, Goldschmidt 2013, 2015, ECROFI 2013, 2015) and 2 times in national (ISZA) conferences. With presentations of our results, Réka Káldos won the first place at the “Meeting of Young Geoscientists” (ISZA) in 2014 and 2015. Further possibility has been arisen making a collaboration with other researchers about Duluth rock samples, using my experience on melt inclusions research from Kerimasi. As a result of this collaboration one paper has been published (*Gál et al., 2014, Ore Geol Rev*). Support of OTKA was noted in all of above mentioned papers.

Raman-FIB-SEM-3D modelling, Kerimasi jacupirangite and afrikandite

An interesting quasi-paradox of carbonatite and alkaline rocks is that the primary alkali minerals are missing, although their presence is expected by experiments (Lee and Wyllie, 1997, 1998a, b; Kjarsgaard, 1998) and natural melt inclusions (Guzmics et al., 2011, 2012, 2015; Mitchell, 2009; Andreeva, 2014, Káldos et al., 2015). Due to intensive alteration (weathering) of these highly water-soluble alkali minerals, analyses of the whole carbonatite rock may provide misleading results and false interpretation about the petrogenesis. However, melt inclusions can preserve the alkali mineral phases. Hence, finding all mineral phases in the melt inclusions is essential to the proper description of formation of carbonatite and alkaline rocks. For this purpose, FIB-SEM technique combined with Raman spectrometry were applied to identify and determine mineral phases in carbonate melt inclusions (n=4) from Kerimasi jacupirangite and afrikandite. Applying Focused Ion Beam (FIB) Scanning Electron Microscopic (SEM) technique in geological/geochemical studies is one of the most promising tool in the last decade (e.g., Dobrzhinetskaya et al., 2001, 2003, 2005; 2006; Heaney et al., 2001; Lee et al., 2003, 2007; Obst et al., 2005; Stöckhert, 2003; Wirth, 2004, 2009; Dégi et al., 2010). It should be noted that only a few works applied FIB-SEM technique in melt inclusion studies. By using FIB-SEM, we can determine the composition and volume ratio of the mineral phases (Dobrzhinetskaya et al., 2003, 2005, 2006; Wirth and Rocholl 2003; Berkesi et al., 2012) present in the melt inclusion and create its 3D model (Anderson and McCarron, 2011). For a more precise determination of the mineral phases in the melt inclusions, we carried out Raman spectroscopic measurements, including 3D Raman mapping on the melt inclusions before FIB-SEM analyses. We performed 320 Raman spectroscopic point measurements on four unexposed and unheated carbonate melt inclusions. During Raman point analyses we identified several mineral phases *e.g.*, perovskite, apatite, phlogopite, carbonates (e.g. calcite, dolomite), alkali carbonates (*e.g.*, nyerereite, shortite, burbankite), sulphates (*e.g.*, sulfohalite, barite) and hydrocarbonate (*e.g.*, nahcolite). Raman mapping was performed on the aforementioned melt inclusions (parallel to the surface of the host mineral and from different confocal depths) with high spatial (step size 0.2 µm horizontally and 1.5 µm vertically) and spectral resolution (Fig 1.). By applying Raman mapping, we obtained the distribution of the identified mineral phases in the melt inclusion in 3D view. As the majority of the melt inclusions are composed of highly water soluble alkali minerals, applying Raman spectroscopy to identify these phases has a particular importance considering that these phases are stable in laser light (Fig 1.). We

performed FIB-SEM analyses on the four previously Raman mapped melt inclusions as well in order to reveal possible Raman inactive phases in the melt inclusions (Fig 2.). FIB-SEM slice-and-view technique was performed on the melt inclusions perpendicular to the surface of the host mineral. Slices were milled in every 200 nanometers, thus the distribution of mineral phases can be observed with extremely high spatial resolution (1-4 nm) including those, which are Raman inactive (e.g. salts) (Fig 2.). During exposure of the melt inclusions, FIB-SEM also allowed obtaining EDS spectra therefore we could get chemical data on each exposed mineral phase as well. There was also an opportunity to take EBSD analyses on each exposed mineral phases of the melt inclusion to support determination of the minerals. Combining these techniques (Raman + FIB-SEM) we could 1/ create a 3D model of the melt inclusion (Fig 3.), hereby 2/ attain the spatial distribution of mineral phases (even submicron sized), and 3/ calculate their volume ratio. We also compared the volume ratios of melt inclusions calculated from Raman maps and FIB-SEM 3D model. The total volume ratio of the melt inclusions calculated from the Raman maps corresponds well to the volume ratios calculated from FIB-SEM 3D model.

Another major goal of our study, beside identification of all mineral phases of the melt inclusions, was to quantify the H_2O (and halogen) content of carbonatite systems. Water plays significant role in polymerization of silicate melts, therefore strongly influence element partitioning between immiscible silicate and carbonate melts (Martin et al., 2012, 2013). Water has not been determined in natural plutonic carbonate melts yet. It should be noted that quenching of dissolved fluid into the carbonate melt phase is not possible (Brooker and Kjarsgaard, 2011, Guzmics et al., 2011, 2012, Káldos et al., 2015), which excludes determining the actual water content of the carbonate melt by analyzing the heated-quenched (in the furnace) and exposed melt phase using in situ analyses (e.g., SIMS.) Moreover, during heating we should consider a possible water loss of the melt due to relatively easy diffusion of this molecule through many host phases (Roedder, 1979; Sobolev et al., 1983; Sobolev and Danyushevsky, 1994). This is why our goal was to study of the daughter minerals in unheated melt inclusions as water (and halogens) are hidden in these minerals. In summary, our coupled Raman spectroscopic and FIB-SEM technique is a powerful tool to determine mineral phases in the melt inclusions in submicron scales and calculate precisely their volume ratio, which allowed us calculating the water content of carbonate melts as well.

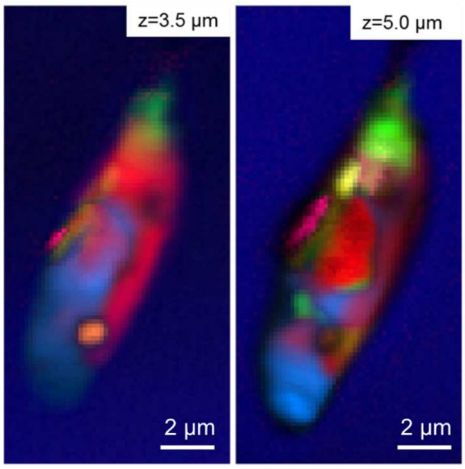

Fig 1: 3D Raman map showing the distribution of mineral phases (mostly alkali carbonates) in two confocal sections in a diopside-hosted carbonate melt inclusion in Kerimasi jacupirangite.

red: alkali carbonate-1, blue: alkali carbonate-2, green: REE-carbonate, yellow: phosphate, orange: oxide, purple: alkali carbonate-3

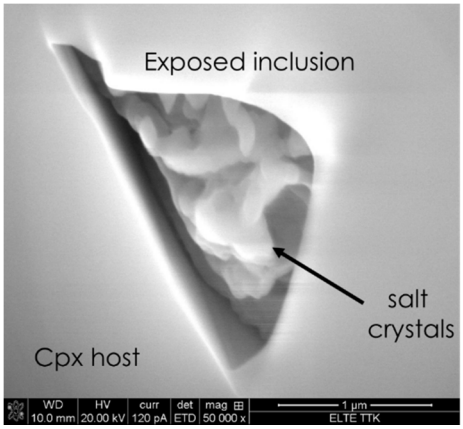

Fig 2: Salt crystals in an opening diopside-hosted carbonate melt inclusion. SE image was taken in the FIB-SEM apparatus.

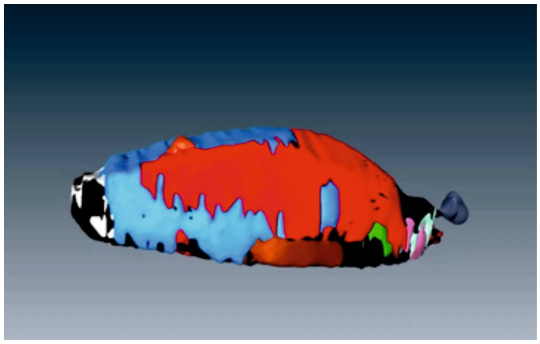

Fig 3: 3D model of a carbonate melt inclusion in Kerimasi jacupirangite created by FIB-SEM apparatus. *red: alkali carbonate-1, blue: alkali carbonate-2, green: REE-carbonate, brown: silicate, orange: oxide-1, pink: carbonate; black: hole; white: salt; grey: oxide-2*

Magnetite carbonatite, Jacupiranga

The studied magnetite carbonatite has cumulate texture and consists of calcite, dolomite, magnetite and phlogopite. The carbonates occur as complex intergrowth of calcite-dolomite and strontianite-calcite. We obtained two textural variations of calcite-dolomite intergrowths 1) an exsolution lamellae of dolomite occurring due to crystallographic orientation of calcite or vice versa 2) randomly distributed dolomite patches appearing in calcite and vice versa.

The calcite, magnetite, phlogopite and dolomite contain multiphase inclusions. Apatite, forsterite, barite, dolomite, calcite, strontianite, geikelite and magnetite occurs as inclusions in phlogopite. Dolomite contains calcite, strontianite, barite, ancylite, Na-Ca carbonate and carboceranite inclusions. Calcite contains dolomite, strontianite, barite, celestine and magnetite inclusions. Magnetite contains dolomite, phlogopite, apatite, barite, geikelite, pyrophanite, baddeleyite, Mg-Al-OH carbonate, chlorite, celestine, strontianite, uranpyrochlore, calcite, sphalerite, Na-Ca carbonate, REE carbonate and vigezzite. Identification of these mineral phases was based on their optical features, EDS spectra and Raman spectroscopic point measurements. The minimum temperature for the rock formation can be estimated as ~900 °C, based on the phase diagram by Goldschmidt (1961) together with the compositions of inter-grown carbonates hosted by magnetite. This data supports magmatic origin of the studied magnetite-carbonatite. The crystallization of the rock can be divided into two periods. 1) In the beginning of crystallization, magnetite-dolomite, forsterite-phlogopite and later on geikelite, apatite, baddeleyite and Mg-Al-OH-carbonate precipitated. 2) This was followed by a significant melt fractionation resulting in formation of Ca-carbonates. In a comparison to other studies (Guzmics et al. 2011, 2012; Mitchell, 2009; Andreeva 2014), the studied magnetite-carbonatite crystallized from a carbonate melt that was richer in MgO than parental carbonate magmas of Kerimasi and Oldoinyo Lengai.

References

Anderson, A., McCarron, T., 2011. Three-dimensional textural and chemical characterization of polyphase inclusions in spodumene using a dual focused ion beamscanning electron microscope (FIB-SEM). Can. Mineral. 49, 541–553.

Andreeva, I.A., 2014. Carbonatitic melts in olivine and magnetite from rare metal carbonatite of the Belaya Zima Alkaline Carbonatite Complex (East Sayan, Russia). Doklady Earth Sciences 455, 436-440.

Berkesi, M., Guzmics, T., Szabó, Cs., Dubessy, J., Bodnar, R.J., Hidas, K. & Ratter, K. (2012) The role of CO_2-rich fluids in trace element transport and metasomatism in the lithospheric mantle beneath the Central Pannonian Basin, Hungary, based on fluid inclusions in mantle xenoliths. Earth and Planetary Science Letters, 331-332, 8–20.

Brooker, R.A., Kjarsgaard, B.A., 2011. Silicate–carbonate liquid immiscibility and phase relations in the system SiO_2–Na_2O–Al_2O_3–CaO–CO_2 at 01–25 GPa with applications to carbonatite genesis. Journal of Petrology 52, 1281-1305.

Dégi, J., Abart, R., Török, K., Bali, E., Wirth, R., Rhede, D., 2010. Symplectite formation during decompression induced garnet breakdown in lower crustal mafic granulite xenoliths: mechanisms and rates. Contrib Mineral Petrol. 159, 293–314.

Dobrzhinetskaya, L.F., Green, H.W., Mitchell, T.E., Dickerson, R.M., 2001. Metamorphic diamonds: mechanism of growth and inclusion of oxides. Geology. 29, 263–266.

Dobrzhinetskaya, L.F., Green, H.W., Weschler, M., Darus, M., Wang, Y.-C., Massonne, H.-J., Stöckhert, B., 2003. Focused ion beam technique and transmission electron microscope studies of microdiamonds from the Saxonian Erzgebirge, Germany. Earth Planet. Sci. Lett. 210, 399–410.

Dobrzhinetskaya, L.F., Wirth, R., Green II., H.W., 2005. Direct observation and analysis of a trapped COH fluid growth medium in metamorphic diamond. TerraNova. 17, 472–477.

Dobrzhinetskaya, L.F., Wirth, R., Green II., H.W., 2006. Nanometric inclusions of carbonates in Kokchetav diamonds from Kazakhstan: a new constraint for the depth of metamorphic diamond crystallization. Earth Planet. Sci. Lett. 243, 85–93.

Gál, B., Molnár, F., Guzmics, T., Aberra, M., Szabó, Cs., Peterson, D.M, 2013. Segregation of magmatic fluids and their potential in the mobilization of platinum-group elements in the South Kawishiwi Intrusion, Duluth Complex, Minnesota - evidence from petrography, apatite geochemistry and coexisting fluid and melt inclusions, Ore. Geol. Rev. 54, 59–80.

Goldsmith, J. R. and Heard, H. C. (1961) Subsolidus phase rclations in the system $CaCO_3$-$MgCO_3$. Journal of Geology, 69, 45- 74.

Guzmics, T., Mitchell, R.H., Szabó, Cs., Berkesi, M., Milke, R., Abart, R., 2011. Carbonatite melt inclusions in coexisting magnetite apatite and monticellite in Kerimasi calciocarbonatite Tanzania: melt evolution and petrogenesis. Contributions to Mineralogy and Petrology 161, 177-196.

Guzmics, T., Mitchell, R.H., Szabó, Cs., Berkesi, M., Milke, R., Ratter, K., 2012. Liquid immiscibility between silicate carbonate and sulfide melts in melt inclusions hosted in co-precipitated minerals from Kerimasi volcano (Tanzania): evolution of carbonated nephelinitic magma. Contributions to Mineralogy and Petrology 164, 101-122.

Guzmics, T., Zajacz, Z., Mitchell, R.H., Szabó, Wälle, M., 2015. The role of liquid–liquid immiscibility and crystal fractionation in the genesis of carbonatite magmas: insights from Kerimasi melt inclusions, Contributions to Mineralogy and Petrology 169, 2015

Heaney, P.J., Vincenzi, E.P., Giannuzzi, L.A., Livi, K.J.T., 2001. Focused ion beam milling: a method of site-specific sample extraction for microanalysis of Earth and planetary materials. Am. Mineral. 86, 1094–1099.

Káldos, R., Guzmics, T., Mitchell, R.H., Dawson, J.B., Milke, R., Szabó, C. (2015) A melt evolution model for Kerimasi volcano, Tanzania: Evidence from carbonate melt inclusions in jacupirangite. Lithos (in press, 10.1016/j.lithos.2015.09.011)

Kjarsgaard, B.A., 1998. Phase relations of a carbonated high CaO nephelinite at 0.2 and 0.5 Gpa. Journal of Petrology 39, 2061-2075.

Lee, M.R., Bland, P.A., Graham, G., 2003. Preparation of TEM samples by focused ion beam (FIB) techniques: applications to the study of clays and phyllosilicates in meteorites. Mineral Mag. 67, 581–592.

Lee, M.R., Brown, D.J., Smith, C.L., Hodson, M.E., MacKenzie, M., Hellmann, R., 2007. Characterization of mineral surfaces using FIB and TEM: a case study of naturally weathered alkali feldspars. Am. Mineral. 92, 1383–1395.

Lee, W.J., Wyllie, P.J., 1997. Liquid immiscibility in the join $NaAlSiO_4$–$NaAlSi_3O_8$–$CaCO_3$ at 1 GPa: Implications for crustal carbonatites. Journal of Petrology 38, 1113-1135.

Lee, W.J., Wyllie, P.J., 1998a. Petrogenesis of carbonatite magmas from mantle to crust, constrained by the system CaO–(MgO+FeO*)–(Na_2O+K_2O)–(SiO_2+Al_2O_3+TiO_2)–CO_2. Journal of Petrology 39, 495-517.

Lee, W.J., Wyllie, P.J., 1998b. Processes of crustal carbonatite formation by liquid immiscibility and differentiation, elucidated by model systems. Journal of Petrology 39, 2005-2013.

Martin, L., Schmidt, M.W., Mattsson, H.B., Ulmer, P., Hametner, K., Günther, D., 2012. Element partitioning between immiscible carbonatite–kamafugite melts with application to the Italian ultrapotassic suite. Chemical Geology 320-321, 96-112.

Martin, L., Schmidt, M.W., Mattsson, H.B., Günther, D., 2013. Element partitioning between immiscible carbonatite and silicate melts for dry and H2O-bearing systems at 1-3 GPa. Journal of Petrology 54, 2301-2338.

Obst, M., Gasser, P., Mavrocordatos, D., Dittrich, M., 2005. TEM-specimen preparation of cell/mineral interfaces by focused ion beam milling. Am. Mineral. 90, 1270–1277.

Roedder, E., 1979. Origin and significance of magmatic inclusions. Bull. Mineral. 102, 487 – 510.

Sobolev, A.V., Danyushevsky, L.V., 1994. Petrology and geochemistry of boninites from the north termination of the Tonga Trench: constraints on the generation conditions of primary high-Ca boninite magmas. J. Petrol. 35, 1183 – 1211

Sobolev, A.V., Clocchiatti, R., Dhamelincourt, P., 1983. Les variations la temperature et de la pression partielle d'eau pendant la cristallisation de l'olivine dans les oceanites du Piton de la Fournaise (Reunion eruption de 1966). C. R. Acad. Sci., Paris 296, 275 – 280.

Stöckhert, B., 2003. Focused ion beam technique and transmission electron microscope studies of microdiamonds from the Saxonian Erzgebirge, Germany. Earth Planet. Sci. Lett. 210, 399–410.

Wirth, R., 2004. Focused Ion Beam (FIB): a novel technology for advanced application of micro-and nanoanalysis in geosciences and applied mineralogy. Eur. J. Mineral. 16, 863–876.

Wirth, R., 2009. Focused Ion Beam (FIB) combined with SEM and TEM: Advanced analytical tools for studies of chemical composition, microstructure and crystal structure in geomaterials on a nanometre scale. Chem. Geol. 261, 217–229.

Wirth, R., Rocholl, A., 2003. Nanocrystalline diamond from the Earth's mantle underneath Hawaii. Earth Planet. Sci. Lett. 211, 357-369.